arXiv:1701.08926v1 [math.AP] 31 Jan 2017

Nonstandard second-order formulation of the LWR model

Wen-Long Jin*

February 1, 2017

Abstract

The seminal LWR model (Lighthill and Whitham, 1955; Richards, 1956) has many equivalent first-order formulations in both Eulerian and Lagrangian coordinates. In this study, we present a second-order formulation of the LWR model based on Phillips' model (Phillips, 1979); but the model is nonstandard with a hyperreal infinitesimal relaxation time. Since the original Phillips model is unstable with three different definitions of stability in both Eulerian and Lagrangian coordinates, we cannot use traditional methods to prove the equivalence between the second-order model, which can be considered the zero-relaxation limit of Phillips' model, and the LWR model, which is the equilibrium counterpart of Phillips' model. Instead, we resort to a nonstandard method based on the equivalence relationship between second-order continuum and car-following models established in (Jin, 2016) and prove that the nonstandard model and the LWR model are equivalent, since they have the same anisotropic car-following model and stability property. We further derive conditions for the nonstandard model to be forward-traveling and collision-free, prove that the collision-free condition is consistent with but more general than the CFL condition (Courant et al., 1928), and demonstrate that only anisotropic and symplectic Euler discretization methods lead to physically meaningful solutions. We numerically solve the lead-vehicle problem and show that the nonstandard second-order model has the same shock and rarefaction wave solutions as the LWR model for both Greenshields and triangular fundamental diagrams; for a non-concave fundamental diagram we show that the collision-free condition, but not the CFL condition, yields physically meaningful results. Finally we present a correction method to eliminate negative speeds and collisions in general second-order models, and verify the method with a numerical example. Together with (Jin, 2016), this study presents a new approach to address the two critiques on second-order continuum models

*Department of Civil and Environmental Engineering, California Institute for Telecommunications and Information Technology, Institute of Transportation Studies, 4000 Anteater Instruction and Research Bldg, University of California, Irvine, CA 92697-3600. Tel: 949-824-1672. Fax: 949-824-8385. Email: wjin@uci.edu. Corresponding author

in (Daganzo, 1995a) and can help to guide the development and discretization of more physically meaningful second-order continuum and car-following models.

Keywords: The LWR model; Phillips' model; hyperreal infinitesimal number; anisotropic and symplectic Euler discretization methods; forward-traveling and collision-free; lead-vehicle problem; correction of second-order models.

1 Introduction

The seminal LWR model describes the evolution of traffic density, $k(t,x)$, speed, $v(t,x)$, and flow-rate, $q(t,x)$ in a time-space domain (Lighthill and Whitham, 1955; Richards, 1956) and can be derived from the following rules (Hereafter we omit (t,x)):

R1. The fundamental law of continuum media: $q = kv$.

R2. The fundamental diagram (Greenshields, 1935): a speed-density relation $v = V(k)$, and a flow-density relation

$$q = \phi(k) \equiv k\eta(k). \tag{1}$$

Here R2 is determined by the static characteristics of traffic flow. Various fundamental diagrams have been proposed. For examples, in the triangular fundamental diagram (Munjal et al., 1971; Haberman, 1977; Newell, 1993), we have:

$$\eta(k) = \min\{V, W(\frac{K}{k} - 1)\}, \tag{2}$$

where V is the free-flow speed, $-W$ characteristic wave speed in congested traffic, K the jam density, and $\tau \equiv \frac{1}{KW}$ is the time gap; in the Greenshields fundamental diagram (Greenshields, 1935), we have

$$\eta(k) \;\; = \;\; V(1 - \frac{k}{K}). \tag{3}$$

R3. Conservation of vehicles:

$$\frac{\partial k}{\partial t} + \frac{\partial kv}{\partial x} = 0. \tag{4}$$

From R1-R3, the LWR model can be written as

$$\frac{\partial k}{\partial t} + \frac{\partial k\eta(k)}{\partial x} \;\; = \;\; 0, \tag{5}$$

which is a scalar hyperbolic conservation law and well-defined with the following two additional implicit rules.

R4. Weak solutions: discontinuous shock waves can develop from smooth initial conditions.

R5. Entropy conditions: certain physical laws are used to pick out unique weak solutions. Traditionally the Lax or Oleinik entropy condition is used to pick out unique solutions (Lighthill and Whitham, 1955; Ansorge, 1990).

Numerically the Godunov method has been successfully applied to solve the LWR model and extended as the Cell Transmission Model for network traffic (Daganzo, 1995b; Lebacque, 1996). Recently, equivalent formulations of the LWR model have been derived with different state variables and coordinate systems. For example, with the cumulative flow as the state variable in Eulerian coordinates, the LWR model is equivalent to a Hamilton-Jacobi equation, which can be solved with the minimum principle in (Newell, 1993) or the variational principle in (Daganzo, 2005). In (Daganzo, 2006), the LWR model was shown to be equivalent to various car-following and cellular automaton models. In (Leclercq et al., 2007), both Hamilton-Jacobi and hyperbolic conservation law formulations of the LWR model were derived and solved in Lagrangian coordinates. In (Laval and Leclercq, 2013), three equivalent Hamilton-Jacobi equations were derived and solved with the Hopf-Lax formula.

It is well known that the LWR model cannot capture scatter and hysteresis in speed- and flow-density relations, spontaneous stop-and-go traffic caused by instability, or bounded acceleration. These limitations have motivated many extensions of the LWR model, including second-order models (e.g. Payne, 1971; Whitham, 1974; Zhang, 1998; Aw and Rascle, 2000; Zhang, 2002; Lebacque, 2003). In these models, the conservation equation, (4), is complemented by an additional equation for the acceleration process. For examples, the acceleration equation in Zhang's model (Del Castillo et al., 1994; Zhang, 1998) can be written as

$$v_t + vv_x = \frac{\eta(k) - v}{T} - (\eta'(k))^2 k k_x, \tag{6}$$

where T is the relaxation time. Such a second-order model reduces to the LWR model, (5), in equilibrium (or steady) states and is traditionally studied as a system of hyperbolic conservation laws with relaxation. It was shown in (Li, 2000) that Zhang's model is stable and converges to the LWR model, when the relaxation time T converges to zero (Liu, 1987). That is, the LWR model is the zero-relaxation limit of Zhang's model.

In this study, we present a nonstandard second-order formulation of the LWR model based on Phillips' model (Phillips, 1979), in which the acceleration equation without the anticipation term is simpler than Zhang's model:

$$v_t + vv_x = \frac{\eta(k) - v}{T}. \tag{7}$$

In particular, we replace the relaxation time by an infinitesimal number, which equals the time step-size in numerical solutions. The formulation is nonstandard, since the infinitesimal relaxation time is a hyperreal number in the nonstandard analysis (Robinson, 1996). The second-order formulation offers a number of advantages over the LWR model: non-equilibrium

initial data can be incorporated, and the acceleration rate can be explicitly calculated, even though it can be a hyperreal number. The second advantage is especially helpful if one introduces bounded acceleration rates into the model.

Furthermore, the method that we employ to analyze and solve the nonstandard second-order model is also nonstandard. In particular, we resort to the equivalence relationship between second-order continuum and car-following models established in (Jin, 2016): we first convert a second-order continuum model into a time- and vehicle-continuous car-following model in Lagrangian coordinates, and then apply the anisotropic method to discretize derivatives in vehicles, and a symplectic Euler method to discretize the acceleration rate and speed in time. Then with their equivalent car-following models, we establish the equivalence between the nonstandard second-order model and the LWR model. We also analytically and numerically solve various lead-vehicle problems, in which the leading vehicle travels at a constant speed, to examine other properties of the model; in particular, we are interested in whether the model is stable, forward-traveling, or collision-free.

The choice of the nonstandard method is prompted by the failure of standard methods for analyzing and solving second-order models.

- First, even though the nonstandard second-order formulation can be considered a zero-relaxation limit of Phillips' model, the traditional approach to proving the equivalence between the zero-relaxation limit (the nonstandard second-order formulation) and the equilibrium model (the LWR model) fails to apply, since Phillips' model is always unstable, as will be proved in Section 2.2. In contrast, with the nonstandard method, we can demonstrate that the nonstandard second-order model and the LWR model have the same car-following model and, therefore, are equivalent.

- Second, traditionally second-order continuum models have been analyzed and solved as systems of hyperbolic conservation laws with relaxation (Liu, 1987). But this approach has led to much confusion regarding the validity of second-order continuum models. For example, in many second-order continuum models, the characteristic wave speeds can be higher than vehicles' speeds; this has led to the conclusion that such models are not anisotropic, as information can travel faster than vehicles (Daganzo, 1995a). However, it was shown in (LeVeque, 2001) that, in the LWR model for night traffic, the characteristic wave speed can also be larger than vehicles' speeds, but anisotropic solutions still exist if one converts the LWR model into a car-following model, except that such anisotropic solutions are different from those obtained with the traditional Oleinik entropy condition for hyperbolic conservation laws. Therefore, we cannot simply conclude that the LWR model with a non-concave fundamental diagram is not anisotropic; rather, when the fundamental diagram is non-concave, we cannot apply the traditional methods to analyze and solve the LWR model as a hyperbolic conservation law. That is, whether characteristic wave speeds are larger than vehicles' speeds is irrelevant to the anisotropy of the LWR model, and the traditional Oleinik and Lax entropy conditions cannot be used to pick out unique, physical solutions.

Since higher-order models have non-equilibrium solutions and much more complicated flow-density relations, we expect that the traditional methods are even less applicable. In contrast, with the nonstandard method, we convert the nonstandard second-order model into a car-following model, as in (LeVeque, 2001), and solve the latter to obtain anisotropic solutions for the former. [1]

- Third, in (Daganzo, 1995a), another issue was raised for second-order models: In an extreme lead-vehicle problem when the leading vehicle is stopped, the following vehicles could travel backwards, and solutions of speeds could be negative. To the best of our knowledge, there is no systematic method to address this critique. In contrast, with the nonstandard method, we will be able to derive conditions to guarantee forward-traveling and collision-free solutions in the car-following model for a second-order continuum model.

The remainder of the paper is organized as follows. In Section 2, we present the nonstandard second-order model and prove that Phillips' model is unstable. In Section 3, we show that the nonstandard second-order model and the LWR model have the same car-following formulation and stability property. In Section 4, we discuss conditions for the nonstandard second-order model to be forward-traveling and collision-free and demonstrate that the anisotropic and symplectic Euler methods are the only physically meaningful discretization methods. In Section 5, we numerically solve the lead-vehicle problem with various fundamental diagrams to verify analytical results. In Section 6, we present a method to correct existing second-order models to eliminate negative speeds and collisions. In Section 7, we conclude the study with further discussions.

2 A nonstandard second-order model

In this section, we first present a nonstandard Phillips' model and then demonstrate that Phillips' model is unstable, both in Eulerian and Lagrangian coordinates. The instability of Phillips' model rules out the traditional method for proving the equivalence between the nonstandard model and the LWR model.

[1] Many efforts have been devoted to addressing Daganzo's first critique regarding anisotropy by developing new models with the characteristic wave speeds not greater than vehicles' speeds (e.g. Aw and Rascle, 2000; Zhang, 2002; Jiang et al., 2002). But we can see that the critique and the ensuing efforts to address it are largely misplaced, since we can obtain anisotropic solutions for all second-order continuum models through their equivalent car-following models, regardless whether their characteristic wave speeds are greater than vehicles' speeds or not.

2.1 Nonstandard Phillips' model

We replace the relaxation time in Phillips' model by an infinitesimal number, ϵ, and obtain the following model:

$$v_t + vv_x = \frac{\eta(k) - v}{\epsilon}, \tag{8}$$

where $\frac{1}{\epsilon}$ is an infinite number. Thus the acceleration rates can be infinite in this model.

Even though infinitesimal and infinite numbers have been used ever since Archimedes' time, especially since Leibniz used infinitesimal numbers in calculus, a rigorous treatment of such numbers was only established after the introduction of hyperreal numbers and nonstandard analysis in 1960's by Robinson (1996). The set of hyperreal numbers is an extension of the set of real numbers by including infinite and infinitesimal numbers. That is, there exists a hyperreal (infinite) number Ω, which is larger than any real number; correspondingly, $\epsilon = \frac{1}{\Omega}$ is a hyperreal (infinitesimal) number and smaller than any positive real number, but greater than 0; and hyperreal numbers can be ordered and satisfy the same addition and multiplication rules for real numbers. For examples, Ω and ϵ can be defined as sequences (Goldblatt, 1998): $\Omega = \langle 1, 2, 3, \cdots \rangle = \langle n : n \in \mathbb{N} \rangle$, and $\epsilon = \langle 1, \frac{1}{2}, \frac{1}{3}, \cdots \rangle = \langle \frac{1}{n} : n \in \mathbb{N} \rangle$ where $\mathbb{N}$ is the set of natural numbers. Hyperreal numbers still form an ordered field as real numbers.

It has been shown that all mathematical arguments in nonstandard analysis can be established in standard analysis. Thus nonstandard analysis is relatively new and not widely studied in the mathematics area. However, infinitesimal/infinite numbers and nonstandard analysis can be very useful for modeling purposes and have been widely used in physics and other areas. For examples, hyperreal numbers have led to simple representations of discontinuous functions, including the Dirac delta function. More importantly they enable the development of nonstandard analysis through intuitive and rigorous interpretations of derivatives and integrals with infinitesimals, which were initiated by Leibniz (Davis, 2005). In (Hanqiao et al., 1986; van den Berg, 1998), nonstandard analysis was applied to solve the heat equation under initial conditions given by a Dirac delta function. In these studies, ϵ is defined as the limit of the time-step size, Δt, and it was shown that ϵ can be simply replaced by Δt in the discrete version of a differential equation and the continuous and discrete equations are equivalent for an infinitesimal Δt.

In this study, we also choose ϵ such that it equals the time-step size, Δt, in the discrete version. In a sense, ϵ is a limit:

$$\epsilon = \lim_{\Delta t \to 0^+} \Delta t, \tag{9}$$

which is an indefinitely small number smaller than any fixed small positive number. In (Jin, 2015a), an indicator function $H(y)$ for $y \geq 0$ was defined as

$$H(y) = \lim_{\Delta t \to 0^+} \frac{y}{\Delta t} = \begin{cases} 0, & y = 0 \\ +\infty, & y > 0 \end{cases}$$

and used in defining both demand and supply functions for the link transmission model. Such an indicator function was also used in formulating the point queue models (Jin, 2015b) and defining a Dirac delta function in (Jin et al., 2016). Thus, $H(y)$ can be represented by the hyperreal number ϵ as

$$H(y) \quad = \quad \frac{y}{\epsilon},$$

or (8) can be re-written with the indicator function

$$v_t + vv_x \quad = \quad H(\eta(k) - v).$$

2.2 Instability of Phillips' model

Phillips' model, (4) and (7), is a system of hyperbolic conservation laws with relaxation, and the LWR model is its equilibrium counterpart. For the system of hyperbolic conservation laws, the two characteristic wave speeds are always identical: $\lambda_1(k, v) = \lambda_2(k, v) = v$. Therefore, it is non-strictly hyperbolic. We denote the characteristic wave speed of the LWR model by $\lambda_*(k) = \phi'(k) = \eta(k) + k\eta'(k)$.

Since nonstandard Phillips' model can be considered as the zero-relaxation limit of Phillips' model, if Phillips' model is stable, then the equivalence between its zero-relaxation limit and the LWR model can be established by following the traditional methods (Liu, 1987; Li, 2000). But in this subsection we demonstrate that Phillips' model is unstable with three different definitions of stability in both Eulerian and Lagrangian coordinates.

Theorem 2.1 *For Phillips' model, its approximate viscous LWR model can be written as*

$$k_t + (k\eta(k))_x \quad \approx \quad -T\frac{\partial}{\partial x}\left((\lambda_*(k) - \eta(k))^2 k_x\right), \tag{10}$$

which is diffusively unstable near an equilibrium state.

Proof. Following (Liu, 1987), we apply the Chapman-Enskog expansion for a small perturbation around an equilibrium state: $v = \eta(k) + v_1$. Here we assume that both v_1 and its derivatives are small; i.e., $v_1 >> \frac{\partial v_1}{\partial x} >> \frac{\partial^2 v_1}{\partial x^2}$ holds for diffusive waves as $t \to \infty$.

Thus (7) can be re-written as

$$\frac{\partial}{\partial t}(\eta(k) + v_1) + \frac{\partial}{\partial x}\left(\frac{1}{2}(\eta(k) + v_1)^2\right) = -\frac{v_1}{T},$$

which can be approximated by

$$v_1 \quad \approx \quad -T\left[\frac{\partial}{\partial t}\eta(k) + \frac{\partial}{\partial x}\frac{1}{2}(\eta(k))^2\right] = -T\eta'(k)(k_t + \eta(k)k_x),$$

by omitting the derivatives of v_1.

Along the characteristic wave direction, we have $\frac{\partial}{\partial t} + \phi'(k)\frac{\partial}{\partial x} \approx 0$, which leads to $k_t \approx -(\eta(k) + k\eta'(k))k_x$. Thus we have

$$v_1 \approx T[\eta'(k)]^2 k k_x,$$

Substituting this into (4), we have

$$k_t + (k\eta(k))_x \approx -T\frac{\partial}{\partial x}((k\eta'(k))^2 k_x),$$

which is equivalent to (10). Since the coefficient of the viscous term is negative, the diffusion process is unstable. ■

Theorem 2.2 *Phillips' model is linearly unstable.*

Proof. We follow (Whitham, 1974, Section 3.1) to prove the linear instability of Phillips' model. We first linearize Phillips' model about an equilibrium state at k_0 and v_0, which satisfy $v_0 = \eta(k_0)$, by assuming $k = k_0 + \kappa$ and $v = v_0 + \nu$, where $\kappa(t, x)$ and $\nu(t, x)$ are small perturbations. Omitting higher-order terms, we have

$$\begin{aligned} \kappa_t + v_0\kappa_x + k_0\nu_x &= 0, \\ \nu_t + v_0\nu_x &= \frac{\eta'(k_0)\kappa - \nu}{T}. \end{aligned}$$

Then we take partial derivatives of the second equation with respect to x and substitute ν_x from the first equation to obtain

$$T\left(\frac{\partial}{\partial t} + v_0\frac{\partial}{\partial x}\right)^2 \kappa = -k_0\eta'(k_0)\frac{\partial \kappa}{\partial x} - \left(\frac{\partial}{\partial t} + v_0\frac{\partial}{\partial x}\right)\kappa.$$

We consider the exponential solution $\kappa = e^{i(mx-\omega t)}$, where m is a real number. The exponential solutions are stable if and only if the imaginary part of ω is negative. Then the above linearized system is equivalent to

$$-T(\omega + mv_0)^2 = -ik_0\eta'(k_0)m + i(\omega + mv_0). \tag{11}$$

The above equation can be rewritten as $\omega^2 + (2b_1 + i2b_2)\omega + (d_1 + id_2) = 0$ with

$$\begin{aligned} 2b_1 &= 2mv_0, \quad 2b_2 = \frac{1}{T}, \\ d_1 &= m^2 v_0^2, \quad d_2 = \frac{v_0 - k_0\eta'(k_0)}{T}m. \end{aligned}$$

According to (Abeyaratne, 2014), both roots of the equation have negative imaginary parts if and only if $b_2 > 0$ and $4b_1b_2d_2 - 4d_1b_2^2 > d_2^2$, or equivalently

$$\begin{aligned} T &> 0, \\ (k_0\eta'(k_0))^2 &< 0, \end{aligned}$$

which is impossible. Therefore Phillips' model is linearly unstable. ■

As shown in (Makigami et al., 1971), the evolution of a traffic stream can be captured by a surface in a three-dimensional space of time t, location x, and vehicle number N. Here the positive direction of x is the same as the traffic direction, and N is the cumulative number of vehicles passing location x at t after a reference vehicle (Moskowitz, 1965). Therefore, N increases in t but decreases in x; i.e., a leader's number is smaller than the follower's. Among these primary three variables, two of them are independent and the other dependent. That is, there exist the following functions:

$$N = n(t, x), \tag{12}$$

$$x = X(t, N). \tag{13}$$

Here (t, x) forms the Eulerian coordinates, and (t, N) the Lagrangian coordinates.

In Eulerian coordinates, $k = -n_x$, and $v = -n_t/n_x$. Transforming all the variables from the Eulerian coordinates into the Lagrangian coordinates, we then have $v = X_t$, $v_t + vv_x = X_{tt}$, and $k = -\frac{1}{X_N}$. Thus Phillips' model can be rewritten as a time- and vehicle-continuous car-following model in the Lagrangian coordinates as

$$X_{tt} = \frac{\theta(-X_N) - X_t}{T}, \tag{14}$$

where

$$\theta(S) = \eta\left(\frac{1}{S}\right) \tag{15}$$

is the speed-spacing relation. For (14), the time-continuous and vehicle-discrete car-following model can be written as

$$X_{tt}(t, N) = \frac{1}{T}\left(\theta\left(\frac{X(t, N - \Delta N) - X(t, N)}{\Delta N}\right) - X_t(t, N)\right), \tag{16}$$

which is the optimal velocity model with an arbitrary ΔN (Bando et al., 1995). Note that, since traffic flow is usually anisotropic and information propagates from the leading vehicle $N - \Delta N$ to the following ΔN, we approximate $-X_N(t, N)$ by $\frac{X(t,N-\Delta N)-X(t,N)}{\Delta N}$ (LeVeque, 2001; Jin, 2016).

Theorem 2.3 *Phillips' model in the Lagrangian coordinates, (14) or (16), is string unstable. That is, a small disturbance in a leading vehicle's speed gets amplified along a traffic stream.*

Proof. We assume that there are small monochromatic disturbances to vehicles' speeds near an equilibrium state with a spacing of s_0 and a speed of v_0, where $s_0 = \theta(s_0)$. Here we denote $X_t(t, N - j\Delta N) = v_0 + \nu_{N-j\Delta N} e^{i\omega t}$ for $j = 0, 1, \cdots, \frac{1}{\Delta N}$. Then $X_{tt}(t, N) = i\omega\nu_N e^{i\omega t}$, and $X(t, N - j\Delta N) = v_0 t + \frac{\nu_{N-j\Delta N}}{i\omega} e^{i\omega t} + X(0, N - j\Delta N)$. Thus, $X(t, N - \Delta N) - X(t, N) = s_0\Delta N + \frac{\nu_{N-\Delta N} - \nu_N}{i\omega} e^{i\omega t}$, where $s_0 = X(0, N-1) - X(0, N)$ is the initial equilibrium spacing. From (16), we have

$$i\omega\nu_N e^{i\omega t} = \frac{1}{T}\left(\theta\left(s_0 + \frac{\nu_{N-\Delta N} - \nu_N}{i\omega\Delta N} e^{i\omega t}\right) - v_0 - \nu_N e^{i\omega t}\right).$$

With the Taylor series expansion of the right-hand side, we obtain

$$i\omega\nu_N e^{i\omega t} \approx \frac{1}{T}\left(\theta'(s_0)\frac{\nu_{N-\Delta N} - \nu_N}{i\omega\Delta N} e^{i\omega t} - \nu_N e^{i\omega t}\right),$$

which leads to

$$i\omega\nu_N \approx \frac{1}{T}\left(\theta'(s_0)\frac{\nu_{N-\Delta N} - \nu_N}{i\omega\Delta N} - \nu_N\right).$$

Thus we have for small ΔN

$$\frac{\nu_N}{\nu_{N-\Delta N}} \approx \frac{\theta'(s_0)}{\theta'(s_0) - T\omega^2\Delta N + i\omega\Delta N} \approx 1 - \frac{1}{\theta'(s_0)}(i\omega - T\omega^2)\Delta N,$$

which leads to by omitting the terms with ΔN^2

$$\left|\frac{\nu_N}{\nu_{N-\Delta N}}\right|^2 \approx 1 + \frac{2T\omega^2\Delta N}{\theta'(s_0)}.$$

Thus we have

$$\left|\frac{\nu_N}{\nu_{N-1}}\right| = \lim_{\Delta N\to 0}\left|\frac{\nu_N}{\nu_{N-\Delta N}}\right|^{\frac{1}{\Delta N}} \approx e^{\frac{T\omega^2}{\theta'(s_0)}}.$$

Since generally speed increases in spacing; i.e., $\theta'(s_0) > 0$, $|\nu_N| > |\nu_{N-1}|$. That is, the following vehicle's speed oscillation magnitude is always larger than the leader's. Therefore a small disturbance in a leading vehicle's speed gets amplified along a traffic stream, and Phillips' model in the Lagrangian coordinates, (14), is string unstable. ■

3 Equivalence and stability

In steady states when the acceleration rate is zero, $v = \eta(k)$ for (4) and (8), and the nonstandard second-order model is equivalent to the LWR model. In this section we prove the equivalence between the nonstandard second-order model and the LWR model under general conditions. We also discuss its stability property.

3.1 Equivalence between the nonstandard second-order model and the LWR model

Here we apply the conversion method developed in (Jin, 2016): we first convert the nonstandard model into equivalent time- and vehicle-continuous car-following model in Lagrangian coordinates, and then discretize the latter into time- and/or vehicle-discrete car-following models.

First, the nonstandard second-order model, (4) and (8), is equivalent to the following time- and vehicle-continuous car-following model in Lagrangian coordinates:

$$X_{tt} = \frac{\theta(-X_N) - X_t}{\epsilon}. \tag{17}$$

Then we discretize X_N in a backward fashion:

$$X_N(t,N) = \frac{X(t,N) - X(t,N-\Delta N)}{\Delta N}. \tag{18}$$

We refer to (18) as an anisotropic method, since, with such a discretization in vehicles, the above model is automatically anisotropic; i.e., the acceleration rate of vehicle N is only impacted by its leading vehicle $N-\Delta N$, but not its following vehicle $N+\Delta N$. Thus the time-continuous and vehicle-discrete car-following model of (17) is

$$X_{tt}(t,N) = \frac{1}{\epsilon}\left(\theta\left(\frac{X(t,N-\Delta N) - X(t,N)}{\Delta N}\right) - X_t(t,N)\right). \tag{19}$$

Furthermore, for a discrete time axis with a time step-size of Δt, both $X_{tt}(t,N)$ and $X(t,N)$ are defined at t, but the speed $X_t(t,N)$ is actually defined at $t-\frac{1}{2}\Delta t$, since it approximates the average speed between t and $t-\Delta t$. Therefore we apply the following explicit and implicit Euler discretization methods for the acceleration rate and speed, respectively, as follows (Jin, 2016):

$$X_{tt}(t,N) = \frac{X_t(t+\Delta t,N) - X_t(t,N)}{\Delta t}, \tag{20a}$$

$$X_t(t+\Delta t,N) = \frac{X(t+\Delta t,N) - X(t,N)}{\Delta t}. \tag{20b}$$

Note that (20) is a symplectic Euler method, if we re-write the time-continuous and vehicle-discrete car-following model, (19), as two Hamiltonian equations for $X(t,N)$ and $X_t(t,N)$ (Hairer et al., 2006, Chapter 6). Setting $\epsilon = \Delta t$, we then obtain the time- and vehicle-discrete car-following model from (19):

$$X_t(t+\Delta t,N) = \theta\left(\frac{X(t,N-\Delta N) - X(t,N)}{\Delta N}\right), \tag{21a}$$

$$X(t+\Delta t,N) = X(t,N) + \Delta t\cdot\theta\left(\frac{X(t,N-\Delta N) - X(t,N)}{\Delta N}\right). \tag{21b}$$

We can see that (21b) is the same as Equation (12) in (Leclercq et al., 2007), derived from the Godunov scheme of the LWR model. Therefore, the nonstandard second-order model, (4) and (8), is equivalent to the LWR model, (5). It is essentially a first-order model but with hyperreal acceleration rates.

3.2 Stability

Theorem 3.1 *The time-continuous and vehicle-discrete car-following model, (19), is linearly stable. That is, a small disturbance in a leading vehicle's speed is not amplified along a traffic stream.*

Proof. Following the proof of Theorem 2.3, we have for small ΔN and ϵ

$$\frac{\nu_N}{\nu_{N-\Delta N}} = \frac{\theta'(s_0)}{\theta'(s_0) - \epsilon\omega^2\Delta N + i\omega\Delta N} \approx 1 - \frac{1}{\theta'(s_0)} i\omega\Delta N,$$

since ϵ is the same order of ΔN. Thus we have

$$\left|\frac{\nu_N}{\nu_{N-\Delta N}}\right|^2 \approx 1 - \frac{\omega^2\Delta N^2}{(\theta'(s_0))^2} < 1,$$

and

$$\left|\frac{\nu_N}{\nu_{N-1}}\right| = \lim_{\Delta N\to 0}\left|\frac{\nu_N}{\nu_{N-\Delta N}}\right|^{\frac{1}{\Delta N}} = 1.$$

Therefore a small disturbance in a leading vehicle's speed is not amplified along a traffic stream, and the nonstandard car-following model, (19), is stable. ■

The stability property of the car-following model is the same as that of the original LWR model.

4 Forward-traveling and collision-free properties

In the preceding section, we demonstrated that, for the nonstandard second-order model, (4) and (8), there exists a unique speed-density relation, its equivalent car-following models, (19), (21a), and (21b), admit anisotropic solutions, and it is stable.

In this section, we discuss two additional properties of the model: forward-traveling and collision-free. We call a model forward-traveling, if vehicles' speeds are always non-negative. We call a model collision-free, if vehicles' spacings are not smaller than the jam spacing, $S \equiv \frac{1}{K}$; i.e., traffic densities are not greater than the jam density. The forward-traveling property was initially introduce in (Daganzo, 1995a) as a criterion to determine the validity of a second-order continuum model. In this study we extend this criterion for car-following models.

4.1 Conditions for forward-traveling and collision-free

In this subsection, we derive conditions for the time- and vehicle-discrete car-following models, (21a) and (21b), to be forward-traveling and collision-free.

Theorem 4.1 *The speed in (21a) is non-negative, if the spacing is not smaller than the jam spacing; i.e., if* $X(t, N-\Delta N) - X(t, N) \geq S\Delta N$. *That is, both (21a) and (21b) are forward-traveling if they are collision-free.*

Proof. For a valid speed-spacing relation, $v = \theta(s)$, the speed is non-negative, if the spacing is not smaller than the jam spacing. Therefore, if $X(t, N-\Delta N) - X(t, N) \geq S\Delta N$, the speed is non-negative. That is, both (21a) and (21b) are forward-traveling if they are collision-free. ■

Note that, for other car-following models, forward-traveling and collision-free properties may be independent of each other. In the following theorem, we derive the sufficient and necessary condition for (21a) and (21b) to be collision-free.

Theorem 4.2 *(21b) is collision-free, if and only if* Δt *and* ΔN *satisfy the following condition:*

$$\frac{\Delta N}{\Delta t} \quad \geq \quad \max_{k\in[0,K]} \frac{\phi(k)}{1-\frac{k}{K}}. \tag{22}$$

Proof. Assuming that the model is collision-free at t; i.e., $X(t, N-\Delta N) - X(t, N) \geq S\Delta N$. At $t + \Delta t$, we have

$$X(t+\Delta t, N-\Delta N) - X(t+\Delta t, N) \quad \geq \quad X(t, N-\Delta N) - X(t+\Delta t, N),$$

where the equal sign holds when the leader, vehicle $N - \Delta N$, suddenly stops. From (21b), we have

$$\begin{aligned} X(t, N-\Delta N) - X(t+\Delta t, N) \quad &= \quad X(t, N-\Delta N) - X(t, N) \\ &\quad -\Delta t \cdot \theta\left(\frac{X(t, N-\Delta N) - X(t, N)}{\Delta N}\right). \end{aligned}$$

Denoting $k = \frac{\Delta N}{X(t,N-\Delta N)-X(t,N)}$, we have

$$X(t, N-\Delta N) - X(t+\Delta t, N) \quad = \quad \frac{\Delta N}{k} - \Delta t\eta(k).$$

Thus the model is always collision-free, if and only if for any $k \in [0, K]$

$$\frac{\Delta N}{k} - \Delta t\eta(k) \geq S\Delta N = \frac{\Delta N}{K},$$

which is equivalent to (22). ■

In (Leclercq et al., 2007), it was shown that (21b) is a Godunov finite difference equation for a hyperbolic conservation formulation of the LWR model in Lagrangian coordinates. For (21b) to be stable, consistent, and, therefore, convergent, the traditional CFL condition (Courant et al., 1928) was derived as

$$\frac{\Delta N}{\Delta t} \quad \geq \quad \max_{k\in[0,K]} |-\eta'(k)k^2|. \tag{23}$$

Clearly the collision-free condition, (22), is not the same as the CFL condition, (23). But we demonstrate that they are equivalent, when the speed-density relation is non-increasing, and the flow-density relation is concave.

Theorem 4.3 *The collision-free condition, (22), is equivalent to the CFL condition, (23), when (i) the speed-density relation is non-increasing; i.e., $\eta'(k) \leq 0$; and (ii) for $k < K$*

$$k\eta''(k) + 2\eta'(k) \leq 0, \tag{24}$$

which is equivalent to the concavity condition for the flow-density relation:

$$\phi''(k) \quad \leq \quad 0. \tag{25}$$

In particular, the two conditions are equivalent for the Greenshields and triangular fundamental diagrams.

Proof. We first assume that the speed-density relation is non-increasing; i.e., $\eta'(k) \leq 0$. This is generally true for many traffic systems, but not for the night traffic system considered in (LeVeque, 2001).

We then assume that (24) is satisfied for $k < K$. It is straightforward to show that (24) is equivalent to (25). From (24) we have $(K-k)(k\eta''(k) + 2\eta'(k)) \leq 0$. Thus $(K-k)k\eta'(k) + K\eta(k)$ is a non-increasing function in k, since its derivative is $(K-k)(k\eta''(k)+2\eta'(k))$. Thus $(K-k)k\eta'(k) + K\eta(k) \geq (K-K)K\eta'(K) + K\eta(K) = 0$. Further we can see that $\frac{\phi(k)}{1-\frac{k}{K}}$ is non-decreasing function, since its derivative is

$$\frac{\phi'(k)(1-\frac{k}{K}) + \phi(k)\frac{1}{K}}{(1-\frac{k}{K})^2} \quad = \quad \frac{(K-k)k\eta'(k) + K\eta(k)}{K(1-\frac{k}{K})^2} \geq 0.$$

Thus (22) is equivalent to $\frac{\Delta N}{\Delta t} \geq \frac{\phi(k)}{1-\frac{k}{K}}|_{k=K} = -\eta'(K)K^2$.

The CFL condition, (23), is equivalent to

$$\frac{\Delta N}{\Delta t} \quad \geq \quad \max_{k\in[0,K]} -\eta'(k)k^2.$$

When (24) is satisfied for $k < K$, then $-\eta'(k)k^2$ is non-decreasing in k, and $\max_{k\in[0,K]} -\eta'(k)k^2 = -\eta'(K)K^2$. Thus (23) is equivalent to $\frac{\Delta N}{\Delta t} \geq -\eta'(K)K^2$.

Therefore, (22) and (23) are equivalent when the speed-density relation is non-increasing, and the flow-density relation is concave.

Then we can show that the Greenshields and triangular fundamental diagrams satisfy the two conditions.

1. For the Greenshields fundamental diagram, (3), we have (i) $\eta'(k) = -\frac{V}{K} < 0$, and (ii) for $k < K$

$$k\eta''(k) + 2\eta'(k) \quad = \quad -\frac{2V}{K} < 0.$$

   Thus,(22) and (23) are equivalent to

$$\frac{\Delta N}{\Delta t} \geq VK. \tag{26}$$

2. For the triangular fundamental diagram, (2), we have (i) $\eta'(k) = 0$ for $k \leq \frac{W}{V+W}K$ and $\eta'(k) = -\frac{WK}{k^2} < 0$ for $k > \frac{W}{V+W}K$, and (ii) for $k < K$

$$k\eta''(k) + 2\eta'(k) \quad = \quad 0.$$

   Thus, (22) and (23) are equivalent to

$$\frac{\Delta N}{\Delta t} \geq WK. \tag{27}$$

■

Note that the CFL condition is derived from the numerical perspective with respect to convergent methods, but the collision-free condition is derived from the physical perspective with respect to safety. The consistence between the collision-free and CFL conditions for normal fundamental diagrams suggests that the physical perspective is meaningful. Further in Section 5, we demonstrate that the collision-free condition is more general and still applies to non-concave fundamental diagrams.

4.2 Other discretization methods

For the time- and vehicle-continuous car-following model, (17), we apply the anisotropic and symplectic Euler discretization methods proposed in (Jin, 2016): (18) for discretizing the spacing in vehicles, and (20) for discretizing the acceleration rate and speed in time. In this subsection, we examine the collision-free property with other discretization methods.

First, we apply the symplectic Euler method to discretize the acceleration and speed in time to obtain the time-discrete and vehicle-continuous form of (17):

$$X(t + \Delta t, N) \quad = \quad X(t, N) + \Delta t \cdot \theta(-X_N(t, N)). \tag{28}$$

But we replace the anisotropic vehicle-discretization method, (18), by one of the following non-anisotropic discretization methods:

1. Forward difference method:

$$X_N(t,N) = \frac{X(t,N+\Delta N)-X(t,N)}{\Delta N}. \tag{29}$$

2. Arithmetic central difference method:

$$X_N(t,N) = \frac{X(t,N+\Delta N)-X(t,N-\Delta N)}{2\Delta N}, \tag{30}$$

   which is the arithmetic average of the backward and forward differences.

3. Harmonic central difference method, which corresponds to the arithmetic central difference method for density (LeVeque, 2001):

$$X_N(t,N) = \frac{2}{\frac{\Delta N}{X(t,N+\Delta N)-X(t,N)}+\frac{\Delta N}{X(t,N)-X(t,N-\Delta N)}}, \tag{31}$$

   which is the harmonic average of the backward and forward differences.

All these discretization methods are non-anisotropic, since the following vehicle's location would impact the leading vehicle's decision. In the following theorem, we demonstrate that such non-anisotropic discretization methods cannot guarantee the collision-free property of the resulted time- and vehicle-discrete car-following models.

Theorem 4.4 *The time- and vehicle-discrete car-following model of (28) with any of the non-anisotropic discretization methods, (29), (30), or (31), is not collision-free, if the speed-density function is greater than zero for any spacing greater than the jam spacing. In other words, it is not safe, if a vehicle determines its speed by looking backwards.*

Proof. We consider an extreme lead-vehicle problem, in which the leading vehicle $N-\Delta N$ stops at an intersection. This corresponds to a red-light scenario. We assume that at t vehicle $N-\Delta N$ is stopped, the spacing between vehicles N and $N-\Delta N$ is $X(t,N-\Delta N)-X(t,N) = S\Delta N$, but the spacing between vehicles $N+\Delta N$ and N is $X(t,N)-X(t,N+\Delta N) > S\Delta N$. So there is no collision at t.

But at $t+\Delta t$ we have from (28)

$$\begin{aligned} X(t+\Delta t,N-\Delta N)-X(t+\Delta t,N) &= X(t,N-\Delta N)-X(t,N)-\Delta t\cdot\theta(-X_N(t,N)) \\ &= S\Delta N-\Delta t\cdot\theta(-X_N(t,N)). \end{aligned}$$

If we use any of the the non-anisotropic discretization methods, (29), (30), or (31), then $-X_N(t,N) > S\Delta N$, which leads to $\theta(-X_N(t,N)) > 0$ for a speed-density function, in which the speed is greater than zero for any spacing greater than the jam spacing. Therefore, $X(t+\Delta t,N-\Delta N)-X(t+\Delta t,N) < S\Delta N$, and vehicle N collides into vehicle $N-\Delta N$. Thus the model is not collision-free.

In addition, the model is not collision-free for other non-anisotropic discretization methods, since $-X_N(t,N)$ would contain the upstream spacing, $\frac{X(t,N+\Delta N)-X(t,N)}{\Delta N}$, and is greater than the jam spacing for the red-light scenario. ■

From the above theorem, we can see that the discretization method in vehicles has to be anisotropic for a model to be collision-free. Even though there can be other anisotropic discretization methods, which can involve multiple leaders, such multiple-leader car-following models are not equivalent to the LWR model.

Next, we apply the anisotropic discretization method for the spacing but use the explicit Euler method to discretize both the acceleration rate and speed in time; i.e., we replace (20) by

$$X_{tt}(t,N) = \frac{X_t(t+\Delta t,N)-X_t(t,N)}{\Delta t}, \tag{32a}$$

$$X_t(t,N) = \frac{X(t+\Delta t,N)-X(t,N)}{\Delta t}. \tag{32b}$$

Thus the corresponding time- and vehicle-discrete car-following model of (17) can be written as

$$X(t+\Delta t,N) = X(t,N)+\Delta t\cdot\theta\left(\frac{X(t-\Delta t,N-\Delta N)-X(t-\Delta t,N)}{\Delta N}\right). \tag{33}$$

In the following theorem, we demonstrate that this model is not collision-free.

Theorem 4.5 *The car-following model, (33), is not collision-free.*

Proof. Again we just need to present one scenario, in which collision can occur at $t+\Delta t$ even though there is no collision at t or $t-\Delta t$.

Consider a red-light scenario: vehicle $N-\Delta N$ is stopped since $t-\Delta t$, $X(t,N-\Delta N)-X(t,N)=S\Delta N$, and $X(t-\Delta t,N-\Delta N)-X(t-\Delta t,N)>S\Delta N$. Then at $t+\Delta t$, we have from (33):

$$\begin{aligned}
X(t+\Delta t,N-\Delta N)-X(t+\Delta t,N) &= X(t,N-\Delta N)-X(t,N)\\
&\quad -\Delta t\cdot\theta\left(\frac{X(t-\Delta t,N-\Delta N)-X(t-\Delta t,N)}{\Delta N}\right)\\
&= S\Delta N\\
&\quad -\Delta t\cdot\theta\left(\frac{X(t-\Delta t,N-\Delta N)-X(t-\Delta t,N)}{\Delta N}\right)\\
&< S\Delta N.
\end{aligned}$$

That is, vehicle N cannot stop at the safe distance and collides into vehicle $N-\Delta N$ at $t+\Delta t$. ■

We can show that the Runge-Kutta and many other discretization methods for the acceleration and speed cannot guarantee the collision-free property of the resulted car-following models. Therefore, the anisotropic and symplectic Euler methods proposed in (Jin, 2016), (18) and (20), appear to be the only physically meaningful methods to discretize the time- and vehicle-continuous car-following model, (17), and (21b) the only physically meaningful car-following model that is equivalent to the nonstandard second-order model, (4) and (8).

5 Numerical examples

In this section, we numerically solve the car-following models of the nonstandard second-order model, (21a) and (21b). We discretize a simulation time duration $[T_0, T_0 + J\Delta t]$ into J intervals and denote $t^j = T_0 + j\Delta t$ $(j = 0, \cdots, J)$. We also divide a plotoon $[0, M\Delta N]$ into M vehicles and denote $N_m = m\Delta N$ $(m = 0, \cdots, M)$. We further denote $U_m^j = X_t(t^j, N_m)$ and $Y_m^j = X(t^j, N_m)$. Then (21a) and (21b) can be respectively rewritten as

$$U_m^{j+1} = \theta\left(\frac{Y_{m-1}^j - Y_m^j}{\Delta N}\right), \tag{34a}$$

$$Y_m^{j+1} = Y_m^j + \Delta t \cdot U_m^{j+1}. \tag{34b}$$

Thus the acceleration rate of vehicle m at $j\Delta t$ is

$$Z_m^j = \frac{U_m^{j+1} - U_m^j}{\Delta t}. \tag{34c}$$

Here we consider the lead-vehicle problem under the following initial and boundary conditions: the boundary conditions are determined by vehicle 0's trajectory $(j \geq 0)$:

$$Y_0^{j+1} = Y_0^j + \Delta t \cdot U_0^{j+1},$$

where $Y_0^0 = 0$, and the leading vehicle's speed $U_0^{j+1} = v_2$ is given and constant; the initial spacings of all following vehicles are constant at $Y_m^0 = -ms_1\Delta N$ for $m = 1, \cdots, M$, where the initial density is $k_1 = 1/s_1$, and their initial speeds are constant at $U_m^0 = v_1 = \eta(k_1)$. Thus the lead-vehicle problem corresponds to a Riemann problem with

$$k(0, x) = \begin{cases} k_1, & x < 0 \\ k_2, & x > 0 \end{cases}$$

where $v_2 = \eta(k_2)$. As we know, the Riemann problem of the LWR model with a concave fundamental diagram is solved by either a shock or a rarefaction wave (Lebacque, 1996). In this section we will compare the numerical results of (34) with the theoretical Riemann solutions.

5.1 Greenshields fundamental diagram

In this subsection we solve the lead-vehicle problem with the Greenshields fundamental diagram, (3), where $S = 7$ m, $K = 1/S$, and $V = 20$ m/s. We set $\Delta t = 0.35\Delta N$, which satisfies the CFL condition and the collision-free condition.

First we set $k_1 = \frac{1}{4}K$, and $v_1 = \frac{3}{4}V$. We consider two cases for the leading vehicle's speed: $v_2 = \frac{3}{8}V$ or $\frac{1}{8}V$; in the Riemann problem, $k_2 = \frac{5}{8}K$ or $\frac{7}{8}K$, respectively. Therefore, the LWR model is solved by a shock wave with a speed of $\frac{1}{8}V$ or $-\frac{1}{8}V$, correspondingly. The numerical solutions of the lead-vehicle problem for (34) are shown in Figure 1, where we show five following vehicles' trajectories and acceleration rates along with the leader's, and the dotted line is the theoretical shock wave trajectory. We show trajectories of each vehicle in figures (a) and (c) from bottom to top for $\Delta N = 1, \frac{1}{2}, \frac{1}{4}, \frac{1}{8}$, and $\frac{1}{16}$; the acceleration rates are from top to bottom with decreasing ΔN. From the figures, we have the following observations: (i) the numerical solutions of the trajectories are smooth, compared with theoretical piecewise linear trajectories; but the deceleration rates are very large; (ii)when ΔN decreases, all vehicles' trajectories converge, and the deceleration rates become larger; (iii) in the converging trajectories, vehicles decrease their speeds immediately after the trajectories cross the shock wave, and the deceleration rates become infinite; (iv) the shock wave speeds are $\frac{1}{8}V$ and $-\frac{1}{8}V$ in figures (a) and (c), respectively, which are exactly the same as the theoretical predictions; the shock waves can also be seen in the propagation of the deceleration profiles in figures (b) and (d). These results verify that the car-following model indeed converges to the LWR model when $\Delta t \to 0$, and the deceleration rates are quite large but can be explicitly calculated.

Next we set $k_1 = K$ and $v_2 = V$. Thus $k_2 = 0$, and there is no vehicle in front of vehicle 0. This is the queue discharge scenario, and the corresponding Riemann problem is solved by a rarefaction wave with the characteristic wave speed spanning from V to $-V$. The first five vehicles' trajectories and acceleration rates are shown in Figure 2, where the dotted line is for the characteristic wave with $\phi'(K) = -V$, along which vehicles start to accelerate one by one. We show the trajectories of each vehicle for $\Delta N = 1, \frac{1}{2}, \frac{1}{4}, \frac{1}{8}$, and $\frac{1}{16}$ from top to bottom; their acceleration rates are from bottom to top. From the figures we can see that the trajectories get closer with smaller ΔN, suggesting that the numerical solutions converge. In addition, vehicles' trajectories become smoother along the traffic stream: the first vehicle has the largest acceleration rates (as large as 53.8 m/s^2 for $\Delta N = \frac{1}{16}$); and the following vehicles' acceleration rates keep decreasing along the vehicles.

5.2 Triangular fundamental diagram

In this subsection we solve the lead-vehicle problem with the triangular fundamental diagram, (2), where $S = 7$ m, $K = 1/S$, $V = 20$ m/s, and $W = 5$ m/s. We set $\Delta t = 1.2\Delta N$, which satisfies the CFL condition and the collision-free condition.

First we set $k_1 = \frac{1}{10}K$, and $v_1 = V$. We consider two cases for the leading vehicle's speed: $v_2 = \frac{3}{8}V$ or $\frac{1}{16}V$. Hence in the Riemann problem $k_2 = \frac{2}{5}K$ or $\frac{4}{5}K$, respectively. In this case,

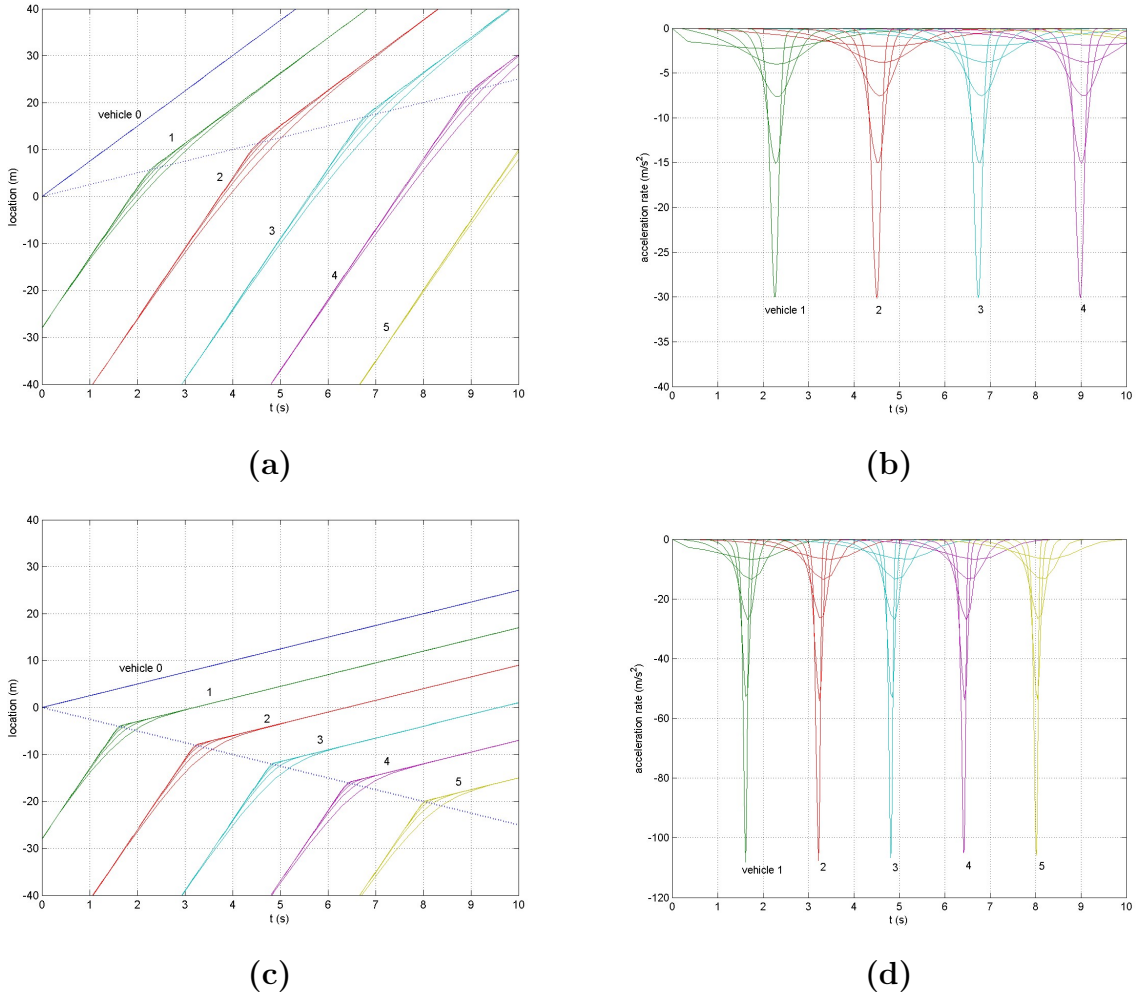

Figure 1: Trajectories and acceleration rates for a platoon of vehicles with $k_1 = \frac{1}{4}K$: (a) Trajectories when $v_2 = \frac{3}{8}V$, (b) Acceleration rates when $v_2 = \frac{3}{8}V$, (c) Trajectories when $v_2 = \frac{1}{8}V$, and (d) Acceleration rates when $v_2 = \frac{1}{8}V$

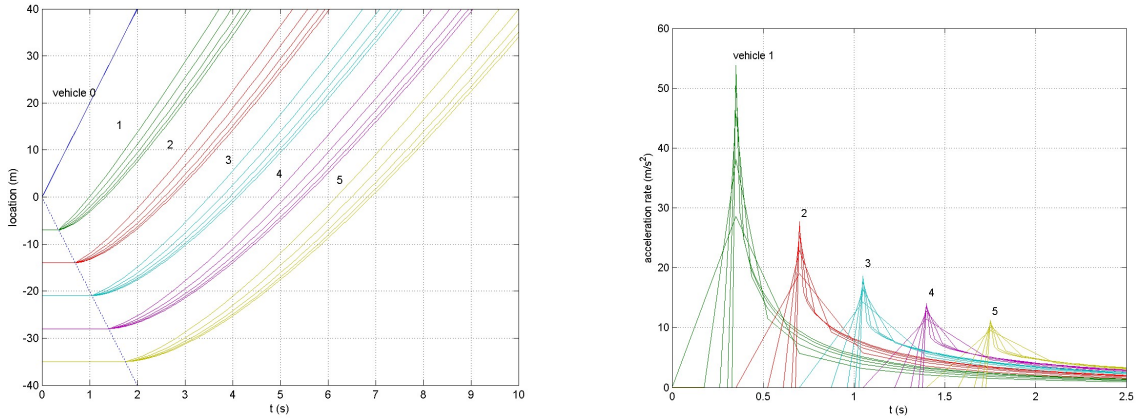

(a) **(b)**

Figure 2: Trajectories and acceleration rates for a platoon of vehicles with $k_1 = K$ and $v_2 = V$

the LWR model is solved by a shock wave with a speed of $\frac{1}{6}V$ or $-\frac{1}{14}V$, correspondingly. The numerical solutions are shown in Figure 3, where we show five following vehicles' trajectories and acceleration rates along with the leader's, and the dotted lines are the theoretical shock wave trajectories. We show trajectories of each vehicle in figures (a) and (c) from bottom to top for $\Delta N = 1, \frac{1}{2}, \frac{1}{4}, \frac{1}{8}$, and $\frac{1}{16}$; the acceleration rates are from top to bottom with decreasing ΔN. From the figures, we have the following observations: (i) in the case of a forward-traveling shock wave, the trajectories are almost the same as the theoretical piecewise linear trajectories for different ΔN; but the deceleration rates increase with smaller ΔN; (ii) in the case of a backward traveling shock wave, the trajectories converge to the theoretical piecewise linear trajectories with decreasing ΔN, and the deceleration rates increase with smaller ΔN; (iii) the shock wave speeds are $\frac{1}{6}V$ and $-\frac{1}{14}V$ in figures (a) and (c), respectively, which are exactly the same as the theoretical predictions; the shock waves can also be seen in the propagation of the deceleration profiles in figures (b) and (d).

Next we set $k_1 = K$ and $v_2 = V$. Thus $k_2 = 0$, and there is no vehicle in front of vehicle 0. This corresponds to the queue discharge scenario, and the corresponding Riemann problem is solved by a degenerate rarefaction wave, which is the same as a shock wave with a speed of $-W$. The first five vehicles' trajectories and acceleration rates are shown in Figure 4, where the dotted line is for the characteristic wave with $\phi'(K) = -W$, along which vehicles start to accelerate one by one. We show trajectories of each vehicle for $\Delta N = 1, \frac{1}{2}, \frac{1}{4}, \frac{1}{8}$, and $\frac{1}{16}$; their acceleration rates are from bottom to top. From the figures we can see that the trajectories are almost identical to the analytical solutions with different ΔN, but the acceleration rates keep increasing with smaller ΔN, and all vehicles' have the same profile for acceleration rates. Thus the numerical solutions converge to theoretical ones for the LWR model, in

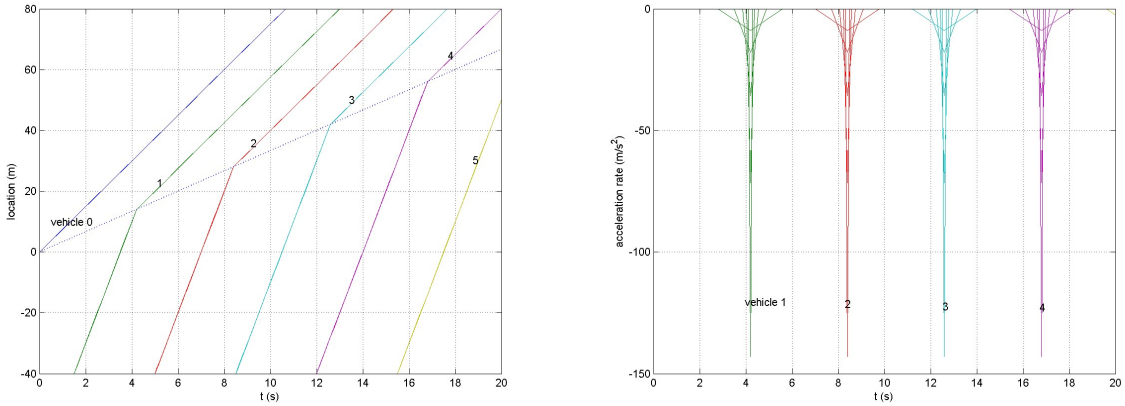

(a) **(b)**

(c) **(d)**

Figure 3: Trajectories and acceleration rates for a platoon of vehicles with the triangular fundamental diagram and $k_1 = \frac{1}{10}K$: (a) Trajectories when $v_2 = \frac{3}{8}V$, (b) Acceleration rates when $v_2 = \frac{3}{8}V$, (c) Trajectories when $v_2 = \frac{1}{16}V$, and (d) Acceleration rates when $v_2 = \frac{1}{16}V$

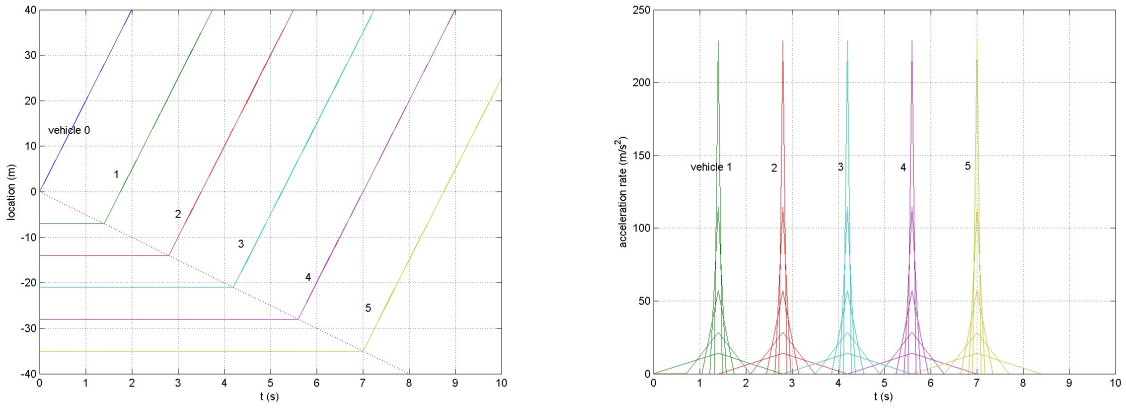

(a) **(b)**

Figure 4: Trajectories and acceleration rates for a platoon of vehicles with $k_1 = K$ and $v_2 = V$

which vehicles accelerate instantaneously, and the acceleration rate is infinite.

5.3 Non-concave fundamental diagram

In this subsection, we solve the lead-vehicle problem with a non-concave fundamental diagram, in which the speed-density relation is given by (Kerner and Konhäuser, 1994): $\eta(k) = 5.0461[(1 + \exp\{[k/K - 0.25]/0.06\})^{-1} - 3.73 \times 10^{-6}]l/T$. Here the unit length $l = 28$ m, the relaxation time $T = 5$ s, and the jam density $K = 0.18$ veh/m. The speed-density relation is decreasing, but the flow-density relation is non-concave.

From the collision-free condition, (22), we have $\frac{\Delta N}{\Delta t} \geq 0.89$, or $\Delta t \leq 1.12\Delta N$; in contrast, from the CFL condition, (23), we have $\frac{\Delta N}{\Delta t} \geq 0.32$, or $\Delta t \leq 3.13\Delta N$. Thus the two conditions are not equivalent for such a non-concave fundamental diagram, and the CFL condition is more relaxed.

In the lead-vehicle problem we set $k_1 = 0.002$ veh/m, and $v_2 = 0$ m/s. Hence $k_2 = K$ in the corresponding Riemann problem. This corresponds to a scenario in which a very sparse traffic stream with a density of 0.002 veh/m runs into a red light. We let $\Delta N = 1/10$.

In Figure 5 we show the numerical results for $\Delta t = \Delta N$, when both the collision-free and CFL conditions are satisfied, and $\Delta t = 2\Delta N$, when the CFL condition is satisfied but the collision-free condition is violated. In the top row with $\Delta t = \Delta N$, the following vehicles' speeds decrease to zero as in figure (b), and the spacings of all following vehicles decrease to the jam spacing of 1/0.18 m, and no collisions occur as in figure (a). But in the bottom row with $\Delta t = 2\Delta N$, when the collision-free condition is violated, vehicles eventually collide into each other as their trajectories overlap in figure (c), and vehicles can develop negative speeds as shown in figure (d). This example confirms the theoretical conclusion that the collision-free

condition is necessary for obtaining physically meaningful solutions in the car-following model, but the CFL condition is no longer sufficient.

6 Correction of general second-order models

In the preceding sections, we established that the time- and vehicle-discrete car-following model, (21b), the nonstandard second-order model, (4) and (8), and the LWR model, (5), are equivalent and have the following properties, under the collision-free condition given in (22): (i) existence of a unique speed-density relation: $v = \eta(k)$; (ii) stable; (iii) anisotropic; (iv) forward-traveling; and (v) collision-free.

In contrast, general second-order models are more realistic than the LWR model, with respect to the instability property and scattered speed-density relations in non-equilibrium traffic. Even though they still admit anisotropic solutions in their equivalent car-following models (Jin, 2016), vehicles may travel backwards, as pointed out in (Daganzo, 1995a). An additional undesirable property is that vehicles may collide into each other in these models. In this section, we present two correction methods to eliminate such unfavorable properties of general second-order models, but keep their favorable ones.

Here we consider general second-order continuum models with the following acceleration equation:

$$v_t + vv_x = \Psi\left(v, \frac{1}{k}, \frac{v_x}{k}\right), \tag{35}$$

in addition to the conservation equation, (4). We assume that, when in equilibrium; i.e., when the speed is both time- and location-independent, the second-order model has a unique speed-density relation, $v = \eta(k)$. That is, $\Psi\left(\eta(k), \frac{1}{k}, 0\right) = 0$. Even though this model doesnot have the anticipation term k_x or the viscosity term v_{xx}, it is sufficiently general to include continuum models in (Phillips, 1979; Greenberg, 2001; Jiang et al., 2002) as well as many converted from car-following models by following the method in (Jin, 2016).

However, as demonstrated in the following subsection, many general second-order continuum models and their corresponding car-following models may have solutions with negative speeds and collisions.

6.1 First correction method

Inspired by the nonstandard second-order model of the LWR model, (4) and (8), we present a correction method to adjust (35) as

$$v_t + vv_x = \max\left\{-\frac{v}{\epsilon}, \min\left\{\frac{\eta(k) - v}{\epsilon}, \Psi\left(v, \frac{1}{k}, \frac{v_x}{k}\right)\right\}\right\}, \tag{36}$$

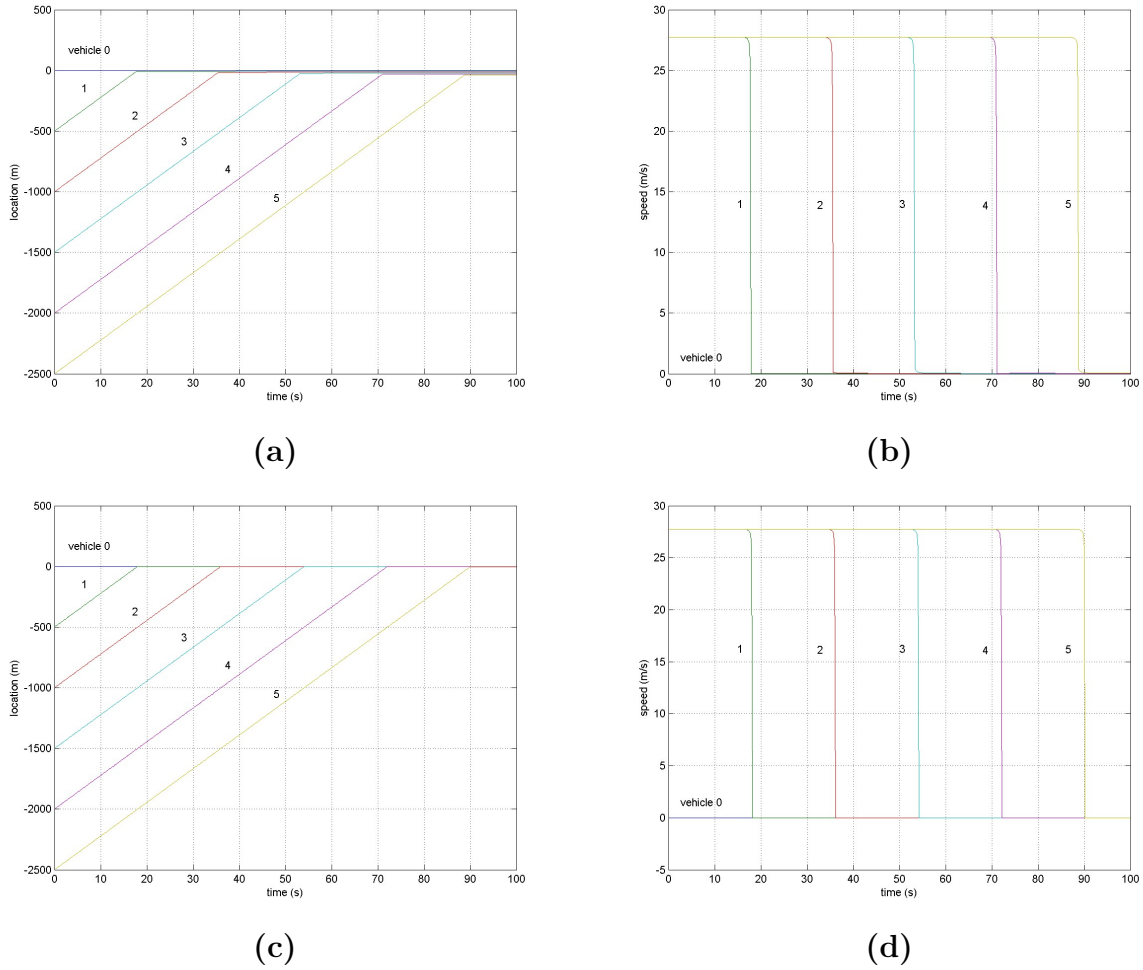

Figure 5: Trajectories and speeds for the LWR model with a non-concave fundamental diagram: In (a) and (b), $\Delta t = \Delta N$ satisfying the collision-free condition; In (c) and (d), $\Delta t = 2\Delta N$ satisfying the CFL condition, but not the collision-free condition

which is equivalent to

$$v_t + vv_x = \min\left\{\frac{\eta(k)-v}{\epsilon}, \max\left\{-\frac{v}{\epsilon}, \Psi\left(v, \frac{1}{k}, \frac{v_x}{k}\right)\right\}\right\}, \tag{37}$$

since $\frac{\eta(k)-v}{\epsilon} \geq -\frac{v}{\epsilon}$. Here we assume that $k \in [0, K]$, and $\eta(k) \geq 0$. We have the following remarks on the correction method:

1. Both of the correction terms, $-\frac{v}{\epsilon}$ and $\frac{\eta(k)-v}{\epsilon}$ contain the hyperreal infinitesimal number ϵ. Thus the corrected model is a nonstandard second-order model, which may not be equivalent to the LWR model.

2. For the corrected model, the speed-density relation in steady states is still $v = \eta(k)$, the same as that for the original model.

3. Among the two correction terms, $-\frac{v}{\epsilon}$ is used to eliminate negative speeds; and $\frac{\eta(k)-v}{\epsilon}$ is the hyperreal acceleration term in the nonstandard second-order formulation of the LWR model, (8), and used to eliminate collisions.

4. In the nonstandard second-order formulation of the LWR model, (4) and (8), the acceleration rate $\Psi(v, \frac{1}{k}, \frac{v_x}{k}) = \frac{\eta(k)-v}{\epsilon}$, and the corrected model is the same as (4) and (8), since $\frac{\eta(k)-v}{\epsilon} \geq -\frac{v}{\epsilon}$. In this sense, the nonstandard second-order formulation, (4) and (8), is already corrected.

Following the conversion method in (Jin, 2016), the corrected second-order model is equivalent to the following second-order car-following model:

$$X_{tt} = \max\left\{-\frac{X_t}{\epsilon}, \min\left\{\frac{\theta(-X_N) - X_t}{\epsilon}, \Psi(X_t, -X_N, -X_{tN})\right\}\right\}, \tag{38a}$$

or

$$X_{tt} = \min\left\{\frac{\theta(-X_N) - X_t}{\epsilon}, \max\left\{-\frac{X_t}{\epsilon}, \Psi(X_t, -X_N, -X_{tN})\right\}\right\}. \tag{38b}$$

Further we discretize the model in vehicle N with the anisotropic and symplectic Euler methods and obtain the time- and vehicle-discrete car-following model:

$$\begin{aligned} X_t(t+\Delta t, N) = \max\Bigg\{0, \min\Bigg\{&\theta\left(\frac{X(t, N-\Delta N) - X(t, N)}{\Delta N}\right), \\ &X_t(t, N) + \Delta t \cdot A(t, N)\Big\}\Bigg\}, \end{aligned} \tag{39a}$$

$$\begin{aligned} X(t+\Delta t, N) = \max\Bigg\{X(t, N), \min\Bigg\{&X(t, N) + \Delta t \cdot \theta\left(\frac{X(t, N-\Delta N) - X(t, N)}{\Delta N}\right), \\ &X(t, N) + \Delta t \cdot X_t(t, N) + \Delta t^2 \cdot A(t, N)\Big\}\Bigg\}. \end{aligned} \tag{39b}$$

where $A(t,N)$ is the acceleration rate in the original second-order model:

$$A(t,N) = \Psi\left(X_t(t,N), \frac{X(t,N-\Delta N)-X(t,N)}{\Delta N}, \frac{X_t(t,N)-X_t(t,N-\Delta N)}{\Delta N}\right). \quad (40)$$

Note that the original acceleration rate is determined by vehicle N's speed, the spacing, and the speed difference.

Theorem 6.1 *When Δt and ΔN satisfy the collision-free condition (22), the corrected car-following models, (39a) and (39b), are forward-traveling and collision-free.*

Proof. From (39a), it is straightforward that $X_t(t+\Delta t, N) \geq 0$; i.e., it is forward-traveling.

From (39b), we have that

$$\begin{aligned} X(t+\Delta t, N-\Delta N) - X(t+\Delta t, N) &\geq X(t, N-\Delta N) - X(t+\Delta t, N) \\ &\geq X(t, N-\Delta N) - X(t, N) \\ &\quad -\Delta t \cdot \theta\left(\frac{X(t,N-\Delta N)-X(t,N)}{\Delta N}\right) \\ &= \frac{\Delta N}{k} - \Delta t \eta(k), \end{aligned}$$

where $k = \frac{\Delta N}{X(t,N-\Delta N)-X(t,N)}$.

If (22) is satisfied, then $\frac{\Delta N}{k} - \Delta t\eta(k) \geq S \cdot \Delta N$, and $X(t+\Delta t, N-\Delta N) - X(t+\Delta t, N) \geq S \cdot \Delta N$. Thus the model is collision-free. ■

6.2 Second correction method

For (35), we present another correction method as

$$v_t + v v_x = \max\left\{-\frac{v}{\epsilon}, \min\left\{(\frac{1}{k}-\frac{1}{K})\frac{\delta}{\epsilon^2} - \frac{v}{\epsilon}, \Psi\left(v, \frac{1}{k}, \frac{v_x}{k}\right)\right\}\right\}, \quad (41)$$

where $\delta = \lim_{\Delta N \to 0^+} \Delta N$ is another infinitesimal number and equal to ΔN in the discrete form.

Following (Jin, 2016), we obtain the following second-order car-following model:

$$X_{tt} = \max\left\{-\frac{X_t}{\epsilon}, \min\left\{(-X_N - S)\frac{\delta}{\epsilon^2}, \Psi(X_t, -X_N, -X_{tN})\right\}\right\}, \quad (42)$$

whose discrete form is

$$\begin{aligned} X_t(t+\Delta t, N) &= \max\left\{0, \min\left\{\frac{X(t,N-\Delta N)-X(t,N)-S\Delta N}{\Delta t}, \right.\right. \\ &\quad \left.\left. X_t(t,N) + \Delta t \cdot A(t,N)\right\}\right\}, \quad (43a) \\ X(t+\Delta t, N) &= \max\left\{X(t,N), \min\left\{X(t,N-\Delta N) - S\Delta N, \right.\right. \\ &\quad \left.\left. X(t,N) + \Delta t \cdot X_t(t,N) + \Delta t^2 \cdot A(t,N)\right\}\right\}. \quad (43b) \end{aligned}$$

where $A(t, N)$ is given in (40).

We have the following observations regarding the second correction method.

1. The second correction method was used to study the optimal velocity model in (Jin, 2016).

2. (43) is forward-traveling and collision-free for any Δt and ΔN.

3. When (22) is satisfied, the speed in the second correction method is greater than or equal to that in the first correction method, since

$$X(t, N - \Delta N) - X(t, N) - \Delta t \cdot \theta \left(\frac{X(t, N - \Delta N) - X(t, N)}{\Delta N} \right) \geq S \Delta N.$$

6.3 An example

In this subsection, we consider the Jiang-Wu-Zhu (JWZ) second-order model (Jiang et al., 2002), in which the original acceleration equation is given by

$$v_t + v v_x = \frac{\eta(k) - v}{T} + c_0 v_x. \tag{44}$$

Thus its two characteristic wave speeds are $\lambda_1(k, v) = v$ and $\lambda_2(k, v) = v - c_0$. If $c_0 \leq 0$, it can be shown that the model is always unstable with the three definitions of stability in Section 2; if $c_0 > 0$, the condition for it to be stable is $-c_0 \leq k\eta'(k) \leq 0$. The corresponding anisotropic car-following model is

$$\begin{aligned} X_t(t + \Delta t, N) &= X_t(t, N) + \Delta t \cdot A(t, N), \\ X(t + \Delta t, N) &= X(t, N) + \Delta t \cdot X_t(t, N) + \Delta t^2 \cdot A(t, N), \end{aligned}$$

where the acceleration rate is given by

$$A(t, N) = \frac{\theta \left(\frac{X(t, N - \Delta N) - X(t, N)}{\Delta N} \right) - X_t(t, N)}{T} + c_0 \frac{X_t(t, N - \Delta N) - X_t(t, N)}{X(t, N - \Delta N) - X(t, N))}.$$

Following the first correction method, we obtain the following corrected, nonstandard second-order continuum model:

$$v_t + v v_x = \max \left\{ -\frac{v}{\epsilon}, \min \left\{ \frac{\eta(k) - v}{\epsilon}, \frac{\eta(k) - v}{T} + c_0 v_x \right\} \right\}, \tag{45}$$

whose car-following formulation is

$$\begin{aligned} X_t(t + \Delta t, N) &= \max \left\{ 0, \min \left\{ \theta \left(\frac{X(t, N - \Delta N) - X(t, N)}{\Delta N} \right), X_t(t, N) + \Delta t \cdot A(t, N) \right\} \right\}, \\ X(t + \Delta t, N) &= \max \Big\{ X(t, N), \min \Big\{ X(t, N) + \Delta t \cdot \theta \left(\frac{X(t, N - \Delta N) - X(t, N)}{\Delta N} \right), \\ &\qquad X(t, N) + \Delta t \cdot X_t(t, N) + \Delta t^2 \cdot A(t, N) \Big\} \Big\}. \end{aligned}$$

We numerically solve the JWZ model and its corrected version for the following Riemann problem studied in (Daganzo, 1995a):

$$(k(0,x), v(0,x)) \quad = \quad \begin{cases} (k_1, 0), & x < 0 \\ (K, 0), & x \geq 0 \end{cases}$$

where k_1 is the upstream initial density. In Lagrangian coordinates, this is the same the red light scenario studied in Section 5.3. In (Daganzo, 1995a), $k_1 = 0$; but to numerically solve the time- and vehicle-discrete version of the JWZ model, we set k_1 to be very small, e.g., $1/100K$, to have vehicles on the upstream part of the road. In Lagrangian coordinates, this corresponds to the following lead vehicle problem: $U_m^0 = 0$ for $m = 0, \cdots, M$, and $Y_m^0 = -ms_1\Delta N$ for $m = 0, \cdots, M$, where $s_1 = 1/k_1$ is the upstream initial spacing. We use the same triangular fundamental diagram as in Section 5.2. In addition, we set $c_0 = 2$ m/s and $T = 5$ s in the JWZ model. In simulations we set $\Delta t = \Delta N = 1$, which satisfies the CFL condition and, equivalently, the absolute collision-free condition.

The trajectories and speeds of the first five vehicles are shown in Figure 6, in which the results in the top row are for the original JWZ model, and those in the bottom row for the corrected JWZ model. In the original model, vehicles first accelerate and eventually stop at a jam spacing; but during the process, vehicles can have negative speeds (see figure (b)) and collide into each other (see figure (a)). Thus the original JWZ model is not always forward-traveling or collision-free, even though it was proved in (Jiang et al., 2002) that there is no negative speeds in a special case when $k_1 = 0$. But both undesirable properties are eliminated in the corrected model (see figures (c) and (d)). Similar results can be observed when we choose other values for c_0, including negative ones. These results validates the proposed correction method.

7 Conclusion

In this study, we present a nonstandard second-order model by replacing the relaxation time in Phillips' model by a hyperreal infinitesimal number. Since Phillips' model is unstable with three different definitions of stability in both Eulerian and Lagrangian coordinates, we cannot use traditional methods based on the assumption of stability to prove the equivalence between the nonstandard model, which can be considered the zero-relaxation limit of Phillips' model, and the LWR model, which is the equilibrium counterpart of Phillips' model. Therefore we resorted to a nonstandard method based on the equivalence relationship between second-order continuum and car-following models in (Jin, 2016) and proved that the nonstandard model and the LWR model are equivalent since they have the same anisotropic car-following model and stability property. We further derived conditions for the car-following model to be forward-traveling and collision-free, proved that the collision-free condition is consistent with the CFL condition for fundamental diagrams with non-increasing speed-density relations and concave flow-density relations, and demonstrated that other discretization methods, including

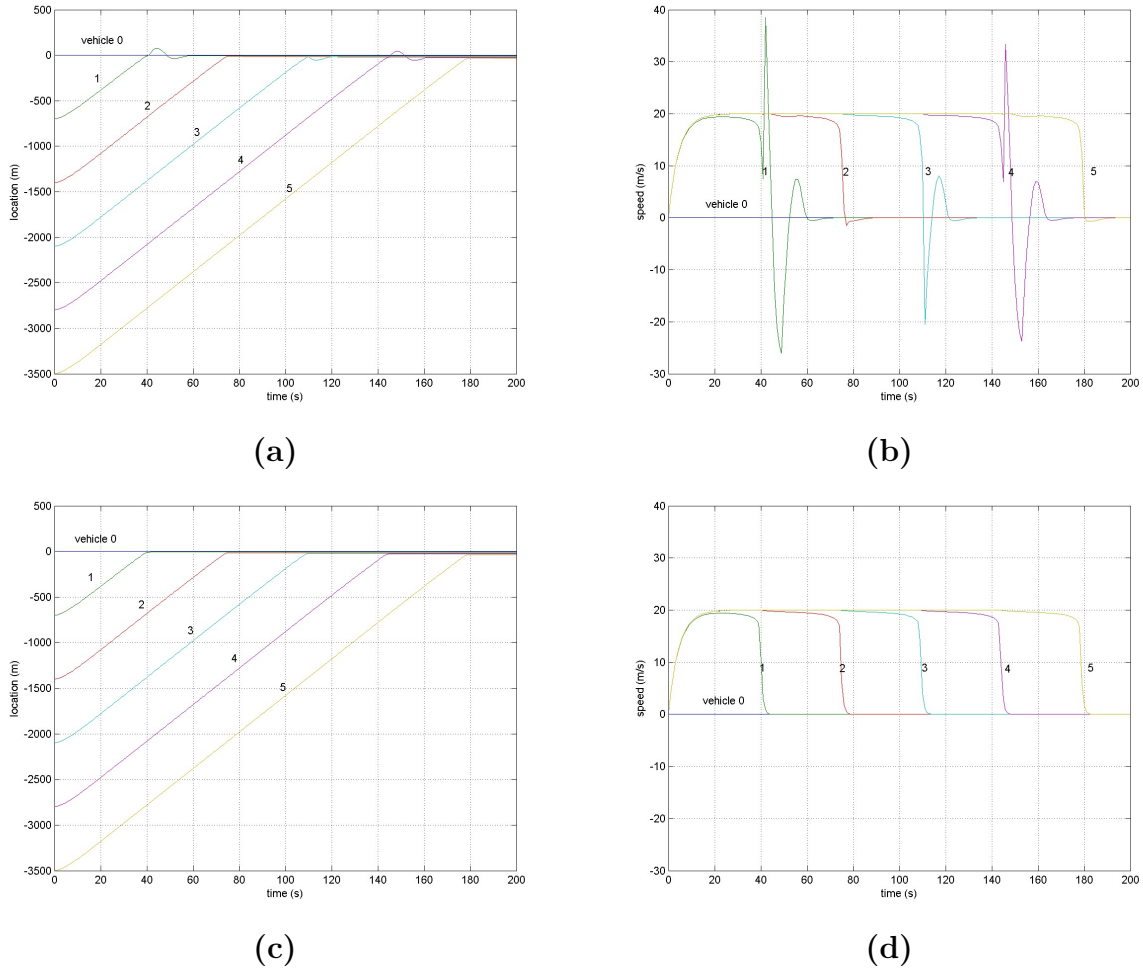

Figure 6: Trajectories and speeds for the JWZ model: (a) & (b) before correction; (c) & (d) after correction method 1

non-anisotropic discretization methods and the explicit Euler method for both the acceleration and speed, will lead to collisions. With numerical solutions to the lead-vehicle problem we showed that the nonstandard second-order model has the same shock and rarefaction wave solutions as the LWR model for both Greenshields and triangular fundamental diagrams; for a non-concave fundamental diagram we showed that the collision-free condition, but not the CFL condition, yields physically meaningful results. Finally we presented a nonstandard method to correct general second-order models so that their solutions are forward-traveling and collision-free, and verified the method with a numerical example.

Theoretical and numerical results in this study further validates the equivalence relationship between higher-order continuum and car-following models established in (Jin, 2016). For hyperbolic conservation laws with non-convex fluxes, non-classical shock wave theories have been developed (Hayes and LeFloch, 1997; LeFloch, 2002). In the same spirit, Oleinik and Lax's entropy conditions should also be revised for the LWR model with non-concave fundamental diagrams or second-order continuum models. In particular, physically meaningful solutions of a continuum model should be consistent with those of the equivalent car-following model. In a sense, the car-following model can serve as an entropy condition to pick out unique and physical solutions for the corresponding continuum model.

In (Jin, 2016), we demonstrated that all second-order continuum models admit anisotropic solutions, through their equivalent car-following models. Therefore, anisotropy is not an intrinsic property of a continuum model, rather it is determined by the discretization method. In this study, we verified that Daganzo's second critique regarding the existence of negative speeds is valid for second-order continuum and car-following models. Moreover, some second-order models are not collision-free. Both undesirable properties were demonstrated for a second-order continuum model and the corresponding car-following model in Section 6.2. However, we showed that all second-order continuum and car-following models can be corrected with the method developed in Section 6.1, so as to eliminate negative speeds and collisions. Therefore, (Jin, 2016) and this study present a new approach to address the two critiques on second-order continuum models in (Daganzo, 1995a): we can follow the correction method and convert them into car-following models to obtain anisotropic solutions that are forward-traveling and collision-free.

In this study, we demonstrated that the nonstandard second-order formulation of the LWR model and, equivalently, the car-following model, have a unique speed-density relation in steady states, is stable, and has anisotropic, forward-traveling, and collision-free solutions. This set of physical properties can serve as conceptual guidelines for analyzing, discretizing, and developing higher-order continuum and car-following models. For example, physically meaningful models and discretization methods should lead to a unique speed-density relation in steady states as well as forward-traveling and collision-free solutions. In particular, the collision-free condition is critical for choosing different discretization methods as well as the time- and vehicle-step sizes; we also demonstrated that it is more general than the CFL condition, which was necessary for converging numerical methods for hyperbolic conservation laws. In particular, such a collision-free condition is critical for developing car-following

algorithms to control connected and automated vehicles. However, the list of physical properties is not complete. In the future we will be interested in introducing upper and lower bounds of the acceleration rate based on the nonstandard second-order formulation of the LWR model as well as the equivalence relationship between continuum and car-following models.

References

Abeyaratne, R. (2014). Macroscopic limits of microscopic models. *International Journal of Mechanical Engineering Education*, 42(3):185--198.

Ansorge, R. (1990). What does the entropy condition mean in traffic flow theory? *Transportation Research Part B*, 24(2):133--143.

Aw, A. and Rascle, M. (2000). Resurrection of "second order" models of traffic flow. *SIAM Journal on Applied Mathematics*, 60(3):916--938.

Bando, M., Hasebe, K., Nakayama, A., Shibata, A., and Sugiyama, Y. (1995). Dynamical model of traffic congestion and numerical simulation. *Physical Review E*, 51(2):1035--1042.

Courant, R., Friedrichs, K., and Lewy, H. (1928). Über die partiellen Differenzengleichungen der mathematischen Physik. *Mathematische Annalen*, 100(1):32--74.

Daganzo, C. F. (1995a). Requiem for second-order fluid approximations of traffic flow. *Transportation Research Part B*, 29(4):277--286.

Daganzo, C. F. (1995b). The cell transmission model II: Network traffic. *Transportation Research Part B*, 29(2):79--93.

Daganzo, C. F. (2005). A variational formulation of kinematic waves: basic theory and complex boundary conditions. *Transportation Research Part B*, 39(2):187--196.

Daganzo, C. F. (2006). In traffic flow, cellular automata= kinematic waves. *Transportation Research Part B*, 40(5):396--403.

Davis, M. (2005). *Applied nonstandard analysis*. Courier Dover Publications.

Del Castillo, J., Pintado, P., and Benitez, F. (1994). The reaction time of drivers and the stability of traffic flow. *Transportation Research Part B*, 28(1):35--60.

Goldblatt, R. (1998). *Lectures on the hyperreals: an introduction to nonstandard analysis*, volume 188. Springer.

Greenberg, J. (2001). Extensions and amplifications of a traffic model of Aw and Rascle. *SIAM Journal on Applied Mathematics*, 62(3):729--745.

Greenshields, B. D. (1935). A study of traffic capacity. *Highway Research Board Proceedings*, 14:448--477.

Haberman, R. (1977). *Mathematical models*. Prentice Hall, Englewood Cliffs, NJ.

Hairer, E., Lubich, C., and Wanner, G. (2006). *Geometric numerical integration: structure-preserving algorithms for ordinary differential equations*, volume 31. Springer Science & Business Media.

Hanqiao, F., St Mary, D., and Wattenberg, F. (1986). Applications of nonstandard analysis

to partial differential equations I. the diffusion equation. *Mathematical Modelling*, 7(2):507--523.

Hayes, B. T. and LeFloch, P. G. (1997). Non-classical shocks and kinetic relations: Scalar conservation laws. *Archive for Rational Mechanics and Analysis*, 139(1):1--56.

Jiang, R., Wu, Q.-S., and Zhu, Z.-J. (2002). A new continuum model for traffic flow and numerical tests. *Transportation Research Part B*, 36(5):405--419.

Jin, W.-L. (2015a). Continuous formulations and analytical properties of the link transmission model. *Transportation Research Part B*, 74:88--103.

Jin, W.-L. (2015b). Point queue models: A unified approach. *Transportation Research Part B*, 77:1--16.

Jin, W.-L. (2016). On the equivalence between continuum and car-following models of traffic flow. *Transportation Research Part B*, 93:543--559.

Jin, W.-L., Recker, W. W., and Wang, X. B. (2016). Instantaneous multihop connectivity of one-dimensional vehicular ad hoc networks with general distributions of communication nodes. *Transportation Research Part B*, 91:159--177.

Kerner, B. S. and Konhäuser, P. (1994). Structure and parameters of clusters in traffic flow. *Physical Review E*, 50(1):54--83.

Laval, J. A. and Leclercq, L. (2013). The hamilton--jacobi partial differential equation and the three representations of traffic flow. *Transportation Research Part B*, 52:17--30.

Lebacque, J. P. (1996). The Godunov scheme and what it means for first order traffic flow models. *Proceedings of the 13th International Symposium on Transportation and Traffic Theory*, pages 647--678.

Lebacque, J. P. (2003). Two-phase bounded acceleration traffic flow model: analytical solutions and applications. *TRB 2003 Annual Meeting*.

Leclercq, L., Laval, J., and Chevallier, E. (2007). The Lagrangian coordinates and what it means for first order traffic flow models. *Transportation and Traffic Theory*, pages 735--754.

LeFloch, P. G. (2002). *Hyperbolic Systems of Conservation Laws: The theory of classical and nonclassical shock waves*. Springer Science & Business Media.

LeVeque, R. J. (2001). Some traffic flow models illustrating interesting hyperbolic behavior. San Diego, CA. SIAM 2001Annual Meeting.

Li, T. (2000). Global solutions and zero relaxation limit for a traffic flow model. *SIAM Journal on Applied Mathematics*, 61(3):1042--1061.

Lighthill, M. J. and Whitham, G. B. (1955). On kinematic waves: II. A theory of traffic flow on long crowded roads. *Proceedings of the Royal Society of London A*, 229(1178):317--345.

Liu, T. P. (1987). Hyperbolic conservation laws with relaxation. *Communications in Mathematical Physics*, 108:153--175.

Makigami, Y., Newell, G. F., and Rothery, R. (1971). Three-dimensional representation of traffic flow. *Transportation Science*, 5(3):302--313.

Moskowitz, K. (1965). Discussion of 'freeway level of service as in uenced by volume and capacity characteristics' by D.R. Drew and C. J. Keese. *Highway Research Record*,

99:43--44.

Munjal, P. K., Hsu, Y. S., and Lawrence, R. L. (1971). Analysis and validation of lane-drop effects of multilane freeways. *Transportation Research*, 5(4):257--266.

Newell, G. F. (1993). A simplified theory of kinematic waves in highway traffic I: General theory. II: Queuing at freeway bottlenecks. III: Multi-destination flows. *Transportation Research Part B*, 27(4):281--313.

Payne, H. J. (1971). Models of freeway traffic and control. *Simulation Councils Proceedings Series: Mathematical Models of Public Systems*, 1(1):51--61.

Phillips, W. (1979). A kinetic model for traffic flow with continuum implications. *Transportation Planning and Technology*, 5(3):131--138.

Richards, P. I. (1956). Shock waves on the highway. *Operations Research*, 4(1):42--51.

Robinson, A. (1996). *Non-standard analysis*. Princeton University Press.

van den Berg, I. P. (1998). On the relation between elementary partial difference equations and partial differential equations. *Annals of pure and applied logic*, 92(3):235--265.

Whitham, G. B. (1974). *Linear and nonlinear waves*. John Wiley and Sons, New York.

Zhang, H. M. (1998). A theory of nonequilibrium traffic flow. *Transportation Research Part B*, 32(7):485--498.

Zhang, H. M. (2002). A non-equilibrium traffic model devoid of gas-like behavior. *Transportation Research Part B*, 36(3):275--290.